Frequency splitter based on the directional emission from surface modes in dielectric photonic crystal structures

Anna C. Tasolamprou,[1,*] Lei Zhang,[2] Maria Kafesaki,[1,3] Thomas Koschny,[2] Costas M. Soukoulis,[1,2]

[1] *Institute of Electronic Structure and Laser, FORTH, 71110, Heraklion, Crete, Greece*
[2] *Ames Laboratory and Department of Physics and Astronomy, Iowa State University, Ames, Iowa 50011, USA*
[3] *Department of Materials Science and Technology, University of Crete, 71003, Heraklion, Crete, Greece*

[*]*atasolam@iesl.forth.gr*

Abstract: We demonstrate the numerical design and the experimental validation of frequency dependent directional emission from a dielectric photonic crystal structure. The wave propagates through a photonic crystal line-defect waveguide, while a surface layer at the termination of the photonic crystal enables the excitation of surface modes and a subsequent grating layer transforms the surface energy into outgoing propagating waves of the form of a directional beam. The angle of the beam is controlled by the frequency and the structure operates as a frequency splitter in the intermediate and far field region.

© 2015 Optical Society of America

OCIS codes: (050.5298) Photonic crystals; (240.6680) Surface plasmons; (050.2770) Gratings.

References and links

1. J. Joannopoulos, P. Villeneuve, and S. Fan, "Photonic crystals: Putting a new twist on light," Nature **386**, 143–149 (1997).
2. S. Johnson, S. Fan, P. Villeneuve, J. Joannopoulos, and L. Kolodziejski, "Guided modes in photonic crystal slabs," Phys. Rev. B **60**, 5751–5758 (1999).
3. E. N. Economou, "Surface plasmons in thin films," Phy. Rev. **182**, 539–554 (1969).
4. S. Maier, M. Brongersma, P. Kik, S. Meltzer, A. Requicha, and H. Atwater, "Plasmonics - a route to nanoscale optical devices," Adv. Mater. **13**, 1501–1505 (2001).
5. D. Gramotnev and S. Bozhevolnyi, "Plasmonics beyond the diffraction limit," Nat. Photonics **4**, 83–91 (2010).
6. P. Kramper, M. Agio, C. M. Soukoulis, A. Birner, F. Müller, R. B. Wehrspohn, U. Gösele, and V. Sandoghdar, "Highly directional emission from photonic crystal waveguides of subwavelength width," Phys. Rev. Lett. **92**, 113903 (2004).
7. H. J. Lezec, A. Degiron, E. Devaux, R. A. Linke, L. Martin-Moreno, F. J. Garcia-Vidal, and T. W. Ebbesen, "Beaming light from a subwavelength aperture," Science **297**, 820–822 (2002).
8. J. Bravo-Abad, F. Garca-Vidal, and L. Martn-Moreno, "Wavelength de-multiplexing properties of a single aperture flanked by periodic arrays of indentations," Photonics and Nanostruct. **1**, 55–62 (2003).
9. L. Martn-Moreno, F. Garcia-Vidal, H. Lezec, A. Degiron, and T. Ebbesen, "Theory of highly directional emission from a single subwavelength aperture surrounded by surface corrugations," Phys. Rev. Lett. **90**, 167401 (2003).
10. R. D. Meade, K. D. Brommer, A. M. Rappe, and J. D. Joannopoulos, "Electromagnetic bloch waves at the surface of a photonic crystal," Phys. Rev. B **44**, 10961–10964 (1991).
11. G. Arjavalingam, W. Robertson, R. Meade, K. Brommer, A. Rappe, and J. Joannopoulos, "Observation of surface photons on periodic dielectric arrays," Opt. Lett. **18**, 528–530 (1993).
12. F. Ramos-Mendieta and P. Halevi, "Surface modes in a 2d array of square dielectric cylinders," Solid State Commun. **100**, 311–314 (1996).

13. S. Xiao, M. Qiu, Z. Ruan, and S. He, "Influence of the surface termination to the point imaging by a photonic crystal slab with negative refraction," Appl. Rev. Lett. **85**, 4269–4271 (2004).
14. I. Bulu, H. Caglayan, and E. Ozbay, "Beaming of light and enhanced transmission via surface modes of photonic crystals," Opt. Lett. **30**, 3078–3080 (2005).
15. R. Moussa, B. Wang, G. Tuttle, T. Koschny, and C. Soukoulis, "Effect of beaming and enhanced transmission in photonic crystals," Phys. Rev. B **76**, 235417 (2007).
16. B. Wang, W. Dai, A. Fang, L. Zhang, G. Tuttle, T. Koschny, and C. Soukoulis, "Surface waves in photonic crystal slabs," Phys. Rev. B **74**, 195104 (2006).
17. W. Dai and C. Soukoulis, "Converging and wave guiding of gaussian beam by two-layer dielectric rods," Appl. Rev. Lett. **93**, 201101 (2008).
18. A. Tasolamprou, L. Zhang, M. Kafesaki, T. Koschny, and C. Soukoulis, "Experimentally excellent beaming in a two-layer dielectric structure," Opt. Express **22**, 23147–23152 (2014).
19. S. Morrison and Y. Kivshar, "Engineering of directional emission from photonic-crystal waveguides," Appl. Phys. Lett. **86**, 1–3 (2005).
20. S. Kim, H. Kim, Y. Lim, and B. Lee, "Off-axis directional beaming of optical field diffracted by a single sub-wavelength metal slit with asymmetric dielectric surface gratings," Appl. Phys. Lett. **90**, 051113 (2007).
21. W. Dai and C. Soukoulis, "Control of beaming angles via a subwavelength metallic slit surrounded by grooves," Phys. Rev. B **82**, 045427 (2010).
22. H. Caglayan, I. Bulu, and E. Ozbay, "Off-axis beaming from subwavelength apertures," J. Appl, Phys. **104**, 73108 (2008).
23. J. Liu, R. Pala, F. Afshinmanesh, W. Cai, and M. Brongersma, "A submicron plasmonic dichroic splitter," Nat. Commun. **2**, 525 (2011).
24. H. Caglayan, I. Bulu, and E. Ozbay, "Off-axis directional beaming via photonic crystal surface modes," Appl. Phys. Lett. **92**, 092114 (2008).
25. N. Yu, Q. Wang, and F. Capasso, "Beam engineering of quantum cascade lasers," Laser Photon. Rev. **6**, 24–46 (2012).
26. https://www.comsol.com

1. Introduction

Subwavelength guiding and manipulating light is a challenge that attracts much of the scientific effort, paving the way towards the minimization of electromagnetic components. Photonic Crystals (PC) and metallic structures, that in the optical regime support the propagation of Surface Plasmons Polaritons (SPPs), have proven to be excellent structural elements for the realization of devices that transmit energy below the diffraction limit [1–5]. Apart from the confinement and guidance of electromagnetic energy, the diffraction limit also imposes serious constraints to the beaming properties of the structures, since as it is known from the basic diffraction law, energy exiting from a subwavelength aperture undergoes a strong angular spread to the whole 2π solid angle. The lack of directionality has a negative impact for the integration of optical components in terms of reduced energy coupling. Nevertheless, it has been shown that it is possible to achieve directional emission out of a subwavelength aperture, both in metallic and photonic crystal structures, by introducing surface corrugations in the exit sides of the aperture [6–8]. Beaming from a metallic subwavelength slit surrounded by a finite array of grooves is associated with the excitation of surface modes, i.e. surface plasmon polaritons, and their collective scattering by the side corrugations [9]. Similarly to the surface plasmon polaritons, dielectric photonic crystals have been found to support the propagation of surface states provided that they are properly terminated. This termination consists of a modified dielectric layer placed at the termination of the bulk photonic crystal; the surface modes propagate bound to this surface layer [10–14]. In order to achieve beaming in these dielectric structures, an additional layer, denoted as grating layer, is added after the modified surface layer. The beaming properties of the structures, such as transmission and directionality, depend on the design of the grating layer; various emitting configurations have been investigated theoretically and experimentally [15–19]. Moreover it has been shown that adding a grating layer with different periodicity in the side of an aperture exit can result in off-axis propagation, i.e. bending of the transmitted beam, in both metallic and dieletric structures [20–25]. Beam

steering may be achieved by properly adjusting the design parameters of the grating layer. Exploiting further the conclusions presented in these previous works, in this paper we present the design and the experimental demonstration of a multifunctional dielectric photonic crystal waveguide that operates as a frequency splitter in the intermediate and far field region. Additionally to previous works our design exhibits off-axis propagation at highly separated angles depending on the frequency of operation. The off-axis emission is achieved by introducing gratings of different periodicity in each side of the waveguide aperture and the steering of the beam is achieved by externally tuning the frequency of operation. The structure is designed so as to provide high spectral and spatial separation as well as low channel cross-talk and low return loss; the relevant performance renders the structure a good candidate for frequency and beam spitting applications. These applications involve for example coupling elements with fine tunable alignment function for integrated free space optical circuits, frequency and spatial optical filters, spatial demultiplexers and frequency dependent surface scanners. The dimensions of the photonic crystal parameters and the frequency of operation have been chosen with respect to the available resources for the experimental validation of the operation in the microwave regime. The dielectric nature of the materials involved allows the scaling of the structure for applications in the optical regime.

2. Structure and beam steering investigation in the dielectric photonic crystal waveguide
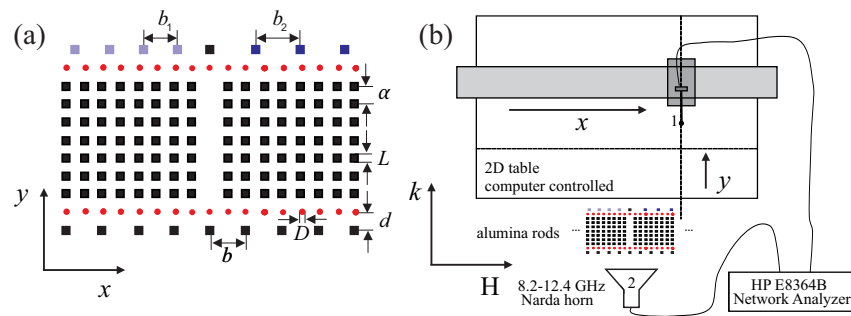

Fig. 1. (a) Schematic of the structure made of square and circular dielectric alumina rods in air. It consists of the input coupling bilayer, the PC waveguide and the output bilayer where the grating layer with the asymmetric side periodicity b_1 and b_2 is located. (b) Experimental configuration. A dipole receiver antenna is used to measure the local field and the emission properties of the structure in the near and intermediate field region. The receiver antenna scans an area of 0.7×0.76 m^2, that is approximately $\sim 23 \times 25\ \lambda^2$.

The proposed PC structure is made of square and circular dielectric alumina rods arranged in air as shown in Fig. 1(a). The dielectric constant of the alumina rods is 9.6. The side length of the square rods is equal to $L = 3.15$ mm and the diameter of the circular rods is equal to $D = 1.83$ mm. The sample is assembled by three sub-elements: an input bilayer which undertakes the coupling of the input field to guided modes, a line-defect PC waveguide which propagates the energy and an output bilayer which forms the shape of the outgoing electromagnetic waves. The input bilayer consists of a grating layer of 19 square rods with lattice constant equal to $b = 22$ mm followed by a surface layer of 37 circular rods with lattice constant matching the bulk PC, $\alpha = 11$ mm. The PC waveguide is formed by removing the central row of a 37×7 square rod bulk PC with lattice constant equal to $\alpha = 11$ mm. Finally the output bilayer is composed of a surface layer, same as the one of the input bilayer, and a grating layer with asymmetric lattice constant b_1 and b_2 in the two exit side directions, $-x$ and $+x$. The vertical y distance between

all the layers is equal to the PC lattice constant, $d = \alpha = 11$ mm. The experimental set-up is presented in Fig. 1(b). It consists of an HP E8364B network analyser, a horn antenna as the transmitter and a dipole antenna as the receiver. The receiver antenna measures the intensity of the local field close to the structure and the propagation, diffraction and interference of the outgoing waves in the near and intermediate field region. The 2D scanning area of the receiver covers the front face at the output bilayer along the lateral (x) direction and extends to 0.76 m, that is $\sim 25\lambda$, along the propagation (y) direction. Pyramidal absorbing panels are placed behind the 2D table to prevent backwards reflection. Additionally, the support for the scanning dipole has been covered with absorber foam to minimize back scattering from the scanning antenna. The numerical investigation of the structure is conducted via the commercial finite element method software COMSOL MULTIPHYSICS [26].

The structure has been designed so as to achieve well defined shape and enhanced transmission for the outgoing waves. The horn antenna transmits a Gaussian beam with TE polarization (the electric field parallel to the dielectric rods $\mathbf{E} \equiv E_z$) at a frequency range of $8.2 - 12.4$ GHz. The mismatch between the horn antenna aperture and the line-defect waveguide width prevents much of the initial energy from coupling into guided modes. Ideally the feeder beam should be of similar width to the waveguide. Amongst the available resources, the input bilayer has been found to better improve the transmission into the structure [15]. The frequency range of interest has been chosen to lie within the photonic bandgap of the bulk PC to ensure localized propagating solutions in the line-defect waveguide and on the surfaces of the PC. The dispersion properties of the bulk PC are calculated via the plane wave expansion method for an infinite periodic structure and are presented in Fig. 2(a). The bangpap of the bulk structure is found at $9.2 - 12.7$ GHz. Finally, the output grating layer modulates the shape of the outgoing waves. The Fabry-Perot cavity, formed between the input and output bilayer, leads to the frequency selective enhancement of the transmitted field.
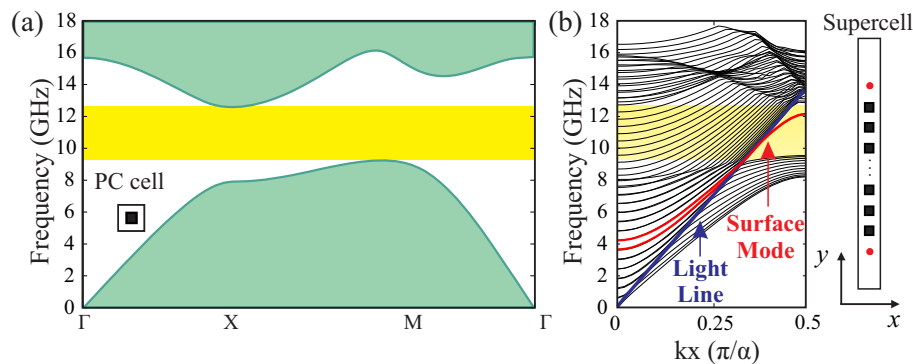

Fig. 2. (a) Bulk photonic crystal dispersion diagram. The dispersion curves are calculated via the plane wave expansion method for the infinite periodic structure. The photonic band gap of the bulk PC lies in the range $9.2 - 12.7$ GHz. (b) Dispersion curves for the finite PC along with the surface layer. They are calculated by applying the plane wave expansion in the supercell shown above. The surface mode dispersion is plotted in red; it lies within the badgap and below the light line (blue curve), and occurs at $10.1 - 12.2$ GHz.

The beam shaping mechanism in the PC structure originates from the excitation and manipulation of surface waves. In the case that the output bilayer were absent, the subwavelength aperture of the PC waveguide would diffract energy in all directions. The corrugated surface layer, made of circular rods, added in the termination of the PC, allows the excitation of surface waves. The surface layer has been designed so as to provide surface modes within the photonic

bandgap and the frequency range under investigation. The dispersion curves of the surface mode are calculated by employing a large enough supercell in the plane wave expansion method. The supercell consists of a finite PC structure with the surface corrugation [14] surrounded by air; it is noted that there is no grating layer in this calculation. Based on the dispersive properties of the surface mode shown in Fig. 2(b), surface propagation it is expected to occur within the range of $10.1 - 12.2$ GHz. The grating layer of the output bilayer, made from differently spaced square rods, facilitates the coupling of the surface modes to outgoing propagating energy and it can be engineered in order to control the angle of the emission. In the case that the grating layer has the same lattice constant in both waveguide sides, $b_1 = b_2$, and under specific conditions, energy diffracted by the grating layer destructively interferes with the waves everywhere, except about the axis of the waveguide, resulting to beaming of the propagating modes in the forward direction. Depending on the asymmetric periods of the grating layer, b_1 and b_2, the direction of the emitted beam changes, which provides control over the angle of the off-axis propagation. Consequently, the first question to be answered is how does the periodicity of the grating layer affects the angle of the emission.
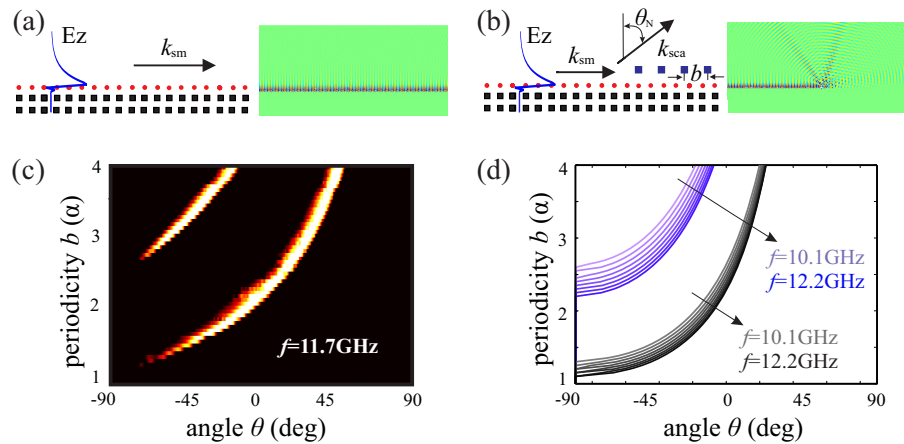

Fig. 3. (a) Schematic of the surface wave propagation along the bulk PC terminated by the surface corrugation. The profile of the E_z component of the TE polarized field and the wavevector k_{sm} are provided by the eigenmode analysis. (b) Schematic of the surface wave propagation along a bulk PC terminated by the surface corrugation with the addition of a grating layer of $b = 3.6\alpha$ at frequency $f = 11.7$ GHz. (c) Angular profile of the propagating waves with respect to the grating layer periodicity b, at frequency $f = 11.7$ GHz, in the intermediate field region as calculated by the full wave calculation. (d) Diffraction angles with respect to the grating layer periodicity b, for frequency ranging from $f = 10.2$ GHz to $f = 11.7$ GHz as calculated by the surface wave and grating equation $k_{sm} \pm Nk_p = k_0 \sin\theta$.

To answer this question, initially we assume that the surface mode propagates along a bulk PC structure terminated by the surface layer as shown in Fig. 3(a). The surface wave is characterized by a parallel wavevector component, k_{sm}, given by the dispersion diagram of the mode presented in Fig. 2(b). The profile of the mode, the E_z component of the TE polarized field, is found by the eigenmode analysis; if the frequency and the geometry remain the same the mode preserves its shape as it propagates, shown in Fig. 3(a). The diffraction phenomena occur when the grating layer interrupts the propagation of the surface mode. The periodic grating layer acts as an array of scatterers and each rod diffracts the incident wave; the collective contribution of all the scatterers leads to the formation of the beams as shown in Fig. 3(b). For the investigation of the impact of the grating layer periodicity b in the beam angle, we performed full wave

numerical calculations using the structure schematically described in Fig. 3(b). The structure is exited at the one side by the surface mode in the specific frequency, here $f = 11.7$ GHz, and the angular profile of the mode is calculated at a radius distance equal to 2 m. The calculation is conducted for variable periodicity b ranging form $b = 1\alpha$ to $b = 4\alpha$. The angular profiles of the outgoing field with respect to the periodicity b are shown in Fig. 3(c). In approximation, the diffraction phenomena can also be described analytically by the surface mode dispersion and the grating equation, $k_{sm} \pm Nk_p = k_0 sin\theta$, where k_{sm} is the wavevector of the surface wave, N an integer, k_p the grating vector and θ the diffraction angle. The analytical calculation of the diffraction orders for variable periodicity b and frequency is presented in Fig. 3(d). The full wave results of Fig. 3(c) and the analytical data of Fig. 3(d) at frequency $f = 11.7$ GHz are similar in quality. As shown, for both calculations, for $b < 1.4\alpha$ there is no diffracted beam, which is consistent with the fact that for these values there are no real solutions for the grating equation. On the other hand, for $b > 3.1\alpha$ we observe the propagation of two diffraction orders which also stands in accordance with the grating equation. Moreover as shown in Fig. 3(d) for a grating layer of constant periodicity higher frequencies favor the generation of second orders of diffraction which provide us a guess for the beaming behavior of the structure. Nevertheless, it should be stressed that the results are not be placed in direct comparison since the surface mode dispersion itself depends on the grating layer which subsequently modifies the angles of the emission. The fact that the similarity of the results is fair should be partially attributed to the fact that as the surface mode meets the grating layer, it is strongly diffracted by the first few scattering rods and then decays rapidly along the propagation direction.

According to the aforementioned physical picture, it is safe to say that the grating equation allows a rough estimation of the direction of the angle depending on the grating periodicity and the frequency of operation. But it is a tool only to be used for an initial estimation and a qualitative interpretation. The selection of the design parameters for the frequency splitter is much more complex than that. Firstly one should take into account that the line-defect waveguide propagating mode is initially, strongly diffracted by the central grating rod. This diffraction apart from producing the surface waves with the $k_\parallel$ component, it also generates waves with variable wavevector direction including the $k_\perp$. In fact there is a tradeoff between the intensity of the generated surface waves and rest of the scattered energy that needs to be balanced. The diffracted waves propagate the guided energy in various directions, they interfere destructively or constructively with the surface-based diffracted waves and contribute to the formation of the outgoing beams. Then one should also have in mind that there are two symmetric surface waves travelling with $k_\parallel$ and $-k_\parallel$ that will suffer diffraction of one or more orders depending on the asymmetric periodicity b_1 and b_2 and the frequency. Each diffraction carries different amount of energy and interferes differently with the rest of the contributions. Finally one should also take into account the additional restrictions imposed in the experimental realization of the structure, that is the finite size of the photonic crystal, the Fabry-Perot between the source antenna and the parts of the structure, the coupling of the energy into the line-defect waveguide. In addition to all these parameters it should be taken into consideration that for the present experiment there are limited choices in terms of rod material and shapes and thus the final design of the frequency splitter is optimized for the specific conditions.

3. The dielectric photonic crystal waveguide as a frequency splitter

The requirement for the operation of a device as a frequency splitter is the ability to shape well defined beams at distinctively different angle propagation and frequency. In order to achieve that for the experiment under consideration, the asymmetric lattice constants have been chosen to be equal to $b_1 = 2.4\alpha$ and $b_2 = 3.6\alpha$ by performing the processes described in the previous section. Figure 4 presents the intensity profile of the outgoing intermediate field at a fixed propagation
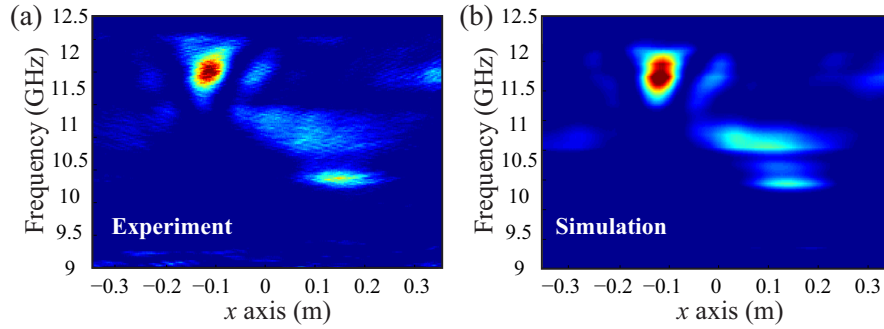
Fig. 4. (a) Experimental x-cross-section profile of the intensity of the intermediate field region within the frequency range of $10 - 12.5$ GHz and (b) corresponding numerical simulation. Axis x is parallel to the surface and grating layer and the intensity is measured/calculated at a fixed point along the propagation axis y, at end of the experimental table ($y_0 = 0.76$ m or $\sim 25\lambda$ away from the sample). Dual band off-axis beaming is observed at frequencies around 10.20 GHz and 11.70 GHz.

point calculated and measured along x axis with respect to the frequency. Axis x is parallel to the grating layer and the measurements and calculations take place at a propagation distance equal to $y = 0.76$ m ($\sim 25\lambda$) from the sample. Figure 4(a) corresponds to the experimental data and Fig. 4(b) to the simulated data. Results indicate that there are two frequency regions, around $f_1 = 11.70$ GHz and $f_2 = 10.20$ GHz, where off-axis directional propagation at different apparent angles is observed. A bright spot also appears at 10.7 GHz which belongs to the frequency evolution of the right going beam. Keeping in mind the estimation results of Fig. 3(d), we observe that as frequency increases the second diffraction orders arise and lead to the formation of the left going beam. The intensity of the outgoing emission in each frequency depends on strength of the surface modes and their coupling to radiation. This is a result of the frequency dependent impedance mismatch in the successive coupling parts and the selective enhancement by the Fabry-Perot waveguide cavity. For our frequency splitter device we aim at the maximum possible spatial and spectral separation and for that reason we choose to focus on frequencies $f_1 = 11.70$ and $f_2 = 10.20$.

The normalized spatial distribution of the outgoing field strength for the two cases is presented in Fig. 5(a-d). Axis x is parallel to the grating layer and axis y perpendicular to the grating layer. Near field region, where evanescent fields are significant and reactance is strong, extends up to the order of a lattice constant/wavelength which is few centimeters away from the exit of the structure. Far field region, where only propagating modes exist, begins after a distance of some tens of lattice constant/wavelength which is a few meters away from the sample. Between the near and far field region lies the intermediate field region where the evanescent field diminishes and interference becomes important. The measurement and simulation results take place at a distance $x = 0.64$ m along the front exit face of the sample and extend to $y = 0.76$ m in the propagation direction, that is the results cover the near field and partially the intermediate field region. Figures 5(a) and 5(b) show the simulated and experimental profiles of the field in the near and intermediate field region for the case of $f_1 = 11.70$ GHz and Fig. 5(c) and 5(d) for the case of $f_2 = 10.20$ GHz. To show more details of the local field in Fig. 5(a-d) the values are separately normalized by their corresponding maximum value. The results demonstrate the bending of the energy by the asymmetric grating layer for the two cases. The diffracted outgoing waves interfere constructively in a certain direction which leads to the formation of the off-axis propagating beams in the intermediate field region. The apparent angular

intensity distribution of the intermediate field at a propagation radius equal to 0.7 m for the two emissions is shown in Fig. 5(e).
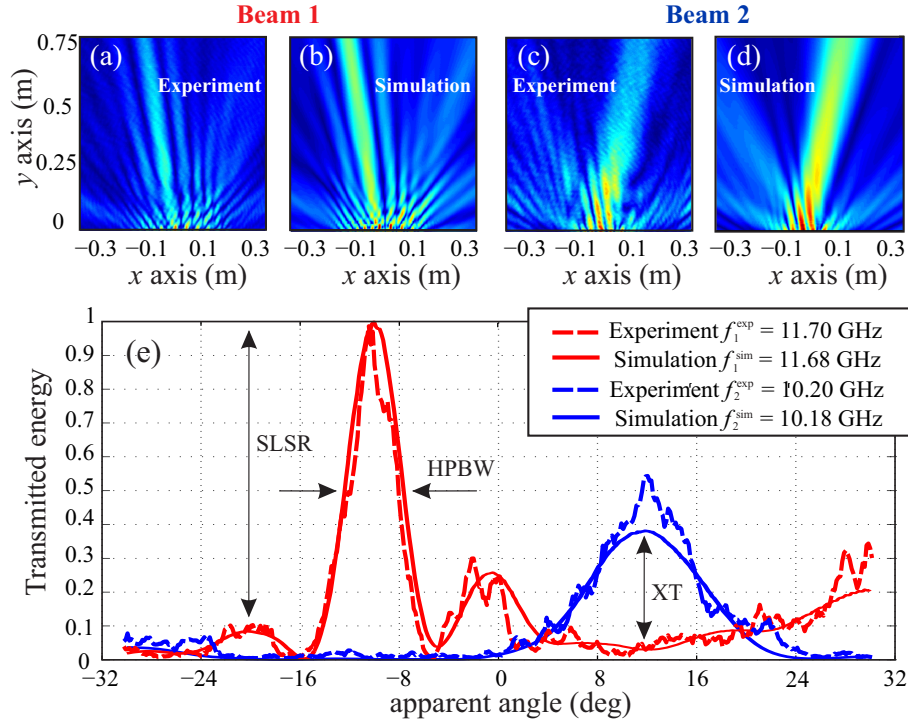

Fig. 5. Experimental (a) and simulated (b) 2D plot of the strength of the outgoing near and intermediate field at frequency $f_1^{exp} = 11.70$ GHz and $f_1^{sim} = 11.68$ GHz. Axis x is parallel to the grating layer and axis y perpendicular to the grating layer. Experimental (c) and simulated (d) 2D plot of the intensity of the outgoing near and intermediate field at frequency $f_2^{exp} = 10.20$ GHz and $f_2^{sim} = 10.18$ GHz. (e) Apparent angular distribution of the beam 1 and 2 at propagation radius equal to 0.7 m. The emerging left going emission, beam 1 propagates along $\phi_1 = -11°$ apparent angular axis and the emerging right going emission, beam 2, along $\phi_2 = +13°$ apparent angular axis.

As presented in Fig. 5(e) in the intermediate field region the structure generates two well defined, Gaussian shaped emissions. The first, left going emission occurs at $f_1 = 11.70$ GHz and it is referred as beam 1. Its main lobe lies at the $\phi_1 = -11°$ angular axis. The full angular width in which the magnitude of the radiation decreases by 3dB, the Half Power Beamwidth (HPBW), is HPBW$_1$=7° and the full 3dB bandwidth is BW$_1$=200 MHz. In this case there appear two side lobes whose generation is connected with the existence of the second diffraction orders at the high frequencies as qualitatively observed in Fig. 3(d). The side lobes lie at angles $-19°$ and $-1°$, that is 8° and 10° away from the main lobe, separation which is sufficiently larger than the half HPBW$_1$. Additionally, as a measurement of the spatial purity of each beam at its main frequency we use the Side Lobe Suppression Ratio (SLSR) which is defined as the ratio of the power of the dominant beam to the power of side lobes. For this case, at $f_1 = 11.70$ GHz, the SLSRs for the two side lobes are quite high, that is 10 dB and 7 dB respectively. The right going emission, referred as beam 2, is found at $f_2 = 10.20$ GHz and propagates along the $\phi_2 = +13°$ angular axis. It is characterized by HPBW$_2 = 10°$ and BW$_2$=500 MHz full 3dB bandwidth. At this frequency no side lodes exist which is related to the fact that at low frequencies there only

exist diffraction of the first order as qualitatively observed in Fig. 3(d). Results show that both the emerging beams are individually well defined in the intermediate field region.

For the frequency splitting operation, the two emerging beams, apart from being individually well defined, they need to be sufficiently separated. Firstly, their angular separation is $\Delta\phi^{intr} = \phi_2 - \phi_1 = 24°$, separation which is sufficiently larger than both the half HPBW$_1$ and HPBW$_2$. Then, their frequency separation is $\Delta f^{intr} = f_1 - f_2 = 1.5$ GHz, separation which is sufficiently larger than both the half BW$_1$ and BW$_2$. The overlap of the the beams is further quantified by the cross-talk (XT), defined as the ratio of the power between the secondary and the dominant beam. Cross-talk remains low for both high and low frequency beams in the corresponding beamwidth, that is XT$_1 < -23$ dB in HPBW$_1$ and XT$_2 < -11$ dB in HPBW$_2$. The energy efficiency of the emitter is evaluated in terms of the Return Losses (RL) in the transmission line, that is the waveguide. Return loss is a product of the mismatch between the waveguide and the termination. This mismatch causes some back reflection of the incident wave reducing the energy efficiency of the emitter. As a result of the back reflection, a standing wave is formed in the waveguide characterized by the Voltage Standing Wave Ratio (VSWR) which is the ratio between the maximum to minimum amplitude of the standing wave; VSWR is proportional to the reflection coefficient. At the high frequency operation the Voltage Standing Wave Ratio is VSWR$_1 = 2.37$ which translates into return losses of RL$_1 = -7.8$ dB. At the low frequency operation the corresponding values are VSWR$_2 = 1.8$ and RL$_2 = -10.5$ dB. As a whole, the high spatial and spectral separation, the low cross-talk and the low return losses indicate that the emerging beams are well separated and that the structure may be used in short range ($\sim 25\lambda$) frequency splitting applications, in the intermediate field region.

The design operates sufficiently well as a frequency splitter; nevertheless there some strategies for improving the device. We have already mentioned the possibility of improving the coupling of the input energy in the waveguide with a use of a different transmitter antenna or given the available means, a better input impedance matching component. The main goal though is to increase the ratio of the energy that is couple to the radiation modes with respect to the energy that propagates in the waveguide. Initially one could maximize the intensity of excited surface waves by minimizing the impedance mismatch between the waveguide and the surface layer. This could be achieved by properly adjusting the diffraction at the end of the waveguide or the surface layer itself, possibly with the use of rods with variable dielectric properties or shapes. Then the surface to radiation coupling efficiency and subsequently the profile of the main beams and the intensity of the side lobes could be further engineered by controlling the periodicity of the grating rods and the scattering strength in a more intensive manner. A similar technique has been presented for plasmonic structures where subwavelength grooves of different volumes and periodicities are etched in the sides of a metallic slit. That allows control over both the diffraction direction and the scattering strength [25]. But the aforementioned metallic configurations hold the advantage of allowing increased resolution for the periodicity of the grooves in the continuous surrounding surface and numerous choices for the grooves shape. In our case of the microwave experiment we could have used grating layer with rods of variable periodicity, permittivity, shape and arrangement that could provide different intensity scattering and direction for the diffracted waves but we are strongly restricted to the discrete alumina dielectric rods. In that sense, the choices we made for our design are optimized for the specific experiment.

Besides the intermediate field region investigation, the beam shaping and frequency splitting capabilities of the structure are studied also in the far field region. For this case the splitting operation frequencies that have been optimized for the intermediate field (Fig. 5) need to be reevaluated. The reason is that the behaviour of the outgoing waves is expected to be qualitatively different in the far field region. In the intermediate field region there also exist strongly localized evanescent modes that interfere with the propagating modes and contribute to the dis-
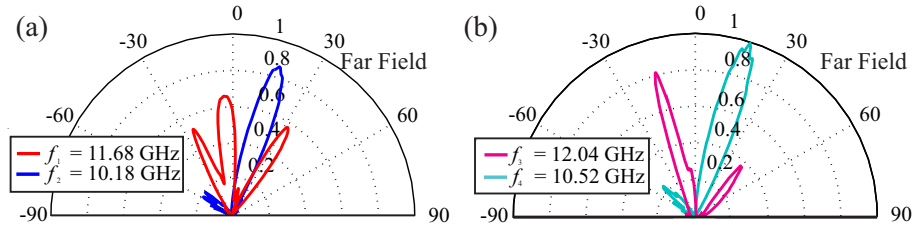
Fig. 6. (a) Far field radiation pattern for the two operation frequencies, $f_1 = 11.7$ GHz and $f_2 = 10.2$ GHz, which optimize beam separation for the frequency splitter in the intermediate field region. (b) Radiation pattern for optimum far field frequency splitting function at $f_3 = 12.04$ GHz and $f_4 = 10.52$ GHz.

tribution of the intermediate field energy. These modes do not survive in the far field region. This is also indicated from Fig. 6(a) where we show the far field radiation pattern for the frequencies that give optimum operation in the intermediate field region. As shown in Fig. 6(a), the high frequency, left going beam splits into three lobes in the far field regime. The main lobe radiates at an angle of $-6°$ with a full HPBW of $9°$. The Side Lobe Suppression Ratio is very low, equal to 0.7 dB and 1.5 dB, but the separation distance between the main and the side lodes is $39°$ and $10°$ respectively. On the other hand, the low frequency, right going beam preserves its near field shape in the far field region. In particular beam 2 in the far field region propagates along the $+19°$ direction with a $15°$ HPBW. Overall, the angular separation of the two beams in the far field region is $25°$ which is sufficiently high; nevertheless the generation of the side lobes in the high frequency degrades the frequency splitting operation.

On the other hand there is a pair of frequencies that exhibit well defined beams, sufficiently high angular and frequency separation in the far field region. As shown in Fig. 6(b), at $f_3 = 12.04$ GHz a beam is formed along $\phi_3 = -14°$ with $\text{HPBW}_3 = 9°$ and $\text{BW}_3 = 550$ MHz. At the same time a second beam is formed at $f_4 = 10.52$ GHz along the $\phi_4 = 19°$ angular axis and it is characterized by $\text{HPBW}_4 = 16°$. This specific beam is quite broadband, with a 3dB full bandwidth of $\text{BW}_4 = 1.5$ GHz. The separation angle, $\Delta\phi^{far} = \phi_4 - \phi_3 = 33°$, is larger than both the half HPBW_3 and HPBW_4 and the separation frequency, $\Delta f^{far} = f_3 - f_4 = 1.52$ GHz, is larger than both the half BW_3 and BW_4. The signal cross-talk remains low for both beams, that is $\text{XT}_3 < -20$ dB in HPBW_3 and $\text{XT}_4 < -14$ dB in HPBW_4. At frequency $f_3 = 12.04$ GHz the VSWR in the transmission line is $\text{VSWR}_3 = 1.4$ that is the return losses are as low as $\text{RL}_3 = -15$ dB and at $f_4 = 10.52$ GHz the corresponding values are $\text{VSWR}_4 = 2.39$ and $\text{RL}_4 = -7.7$ dB. Results indicate the generation of two emissions with high angular and spectral separation, low cross-talk and return losses and prove that the structure can also be used in long range frequency splitting applications for free space emission in the far field.

4. Conclusions

We have demonstrated the design and experimental realization of a multifunctional dielectric photonic crystal structure which can operate both as beam steering device and frequency splitter. In the structure the energy propagates through a line-defect photonic crystal waveguide; a modified surface layer at the termination of the bulk photonic crystal waveguide enables the excitation of surface modes and a rear grating layer couples the surface field to radiating energy. The proper selection of the grating layer design parameters enforces the directional emission of the outgoing wave. The asymmetric periodicity of the grating layer in the two sides leads to the off-axis propagation of the outgoing beam. Beaming along different angles occurs at different frequencies and the structure can be used as constructional element in beam steering and

frequency splitting application both in the intermediate and far field region.

Acknowledgment